Journal of Catalysis **198,** 208–222 (2001)
doi:10.1006/jcat.2000.3111, available online at http://www.idealibrary.com on IDEAL®

WO_3–CeO_2 and Pd/WO_3–CeO_2 as Potential Catalysts for Reforming Applications

I. Physicochemical Characterization Study

C. Bigey,[1] L. Hilaire, and G. Maire

Laboratoire d'Etudes de la Réactivité Catalytique, des Surfaces et Interfaces, UMR 7515 du CNRS, ECPM, 25, rue Becquerel, BP 08, 67087 Strasbourg Cedex 2, France

Received July 7, 2000; revised October 3, 2000; accepted October 28, 2000; published online February 8, 2001

WO_3–CeO_2 (9.1 wt% WO_3) and Pd/WO_3–CeO_2 materials were prepared with a tungsten loading corresponding to a tungsten coverage lower than one theoretical equivalent monolayer. Physicochemical characterizations (N_2 adsorption, X-ray diffraction, Raman spectroscopy, and TPR experiments) allowed us to show that the technique used to prepare the catalyst favors the formation of a dispersed W phase containing tetrahedral tungsten species. We identified the important role of the Na remaining from the tungstate precursor (Na_2WO_4) on the structural evolution of W species. Na^+ strongly bound to the support would prevent the condensation of monomeric WO_4^{2-}, avoiding the formation of polymeric species. We have proposed the existence of various WO_4^{2-} species (monomeric or dimeric), as a function of the adsorption mode for which the tungsten is maintained in the +VI oxidation state. Dehydration treatment leads to WO_4^{2-} species linked to a pair of hydroxyl groups which induces structure distortions. Some WO_3 crystallites are observed after a reduction at 350°C of the WO_3–CeO_2 material which are no longer observed after calcination. The tungstate species are strongly bound to the support and thus hardly reducible. They are reduced around 900°C in one step giving tungsten metal.

Key Words: **tungsten; ceria; palladium; WO_3–CeO_2; XRD; Raman; TPR.**

1. INTRODUCTION

Tungsten-based catalysts supported on oxides (Al_2O_3, TiO_2, SiO_2, ZrO_2) have been used in various processes, namely hydrodesulfurization (1, 2), selective catalytic reduction of NOx (3), and olefins metathesis (4, 5). Acid properties of tungsten-based catalysts have also been employed to improve alkane isomerization, a very important step in the synthesis of high octane rating petrol (6–9). The properties of bulk tungsten oxides (WO_3[2] and WO_2) were studied in hexane reforming (10, 11) and heptane hydrocracking (12). Such research has disclosed two important points. First, pure WO_3 (and WO_2 which is largely oxidized in WO_3 at the surface) is inactive due to the lack of metallic properties. Treatment under H_2 is necessary to produce metallic sites (WO_{3-x}) allowing us to observe catalytic activity. Second, it is a difficult task to obtain stable catalytic properties which are linked to the reduction of tungsten oxides under operating conditions occurring in a multistep process, as shown by means of X-ray photoelectron spectroscopy (XPS) (13–17), temperature-programmed reduction (TPR) (18–20), or thermogravimetric analysis (TGA) (12, 21), leading to a great variety of WO_{3-x} substoichiometric oxides.

Recently, we reported that the addition of palladium to WO_3 or WO_2 bulk oxides could improve the reactivity toward alkanes (22–24). The highest selectivity in isomerized products was observed in the presence of W^{6+} cations. Stable isomerization properties, attributed to the $W_{20}O_{58}$ phase formation (containing W^{5+} and W^{6+} cations), were obtained after further reduction at 350°C. However, the metallic function of palladium was very sensitive to hydrocarbon poisoning, leading to catalyst deactivation toward saturated alkanes. From these results, it appeared necessary to stabilize the oxide and metallic active phases (W^{6+} cations, Pd) which confer acidic and metallic properties for isomerization and hydro-dehydrogenation reactions. The use of a support seemed to be a potential way. Indeed, some previous formulations, such as Pt/WOx–ZrO_2 (25–30), Pt- or Ni/WO_3–Al_2O_3 (31, 32), or Pt/WO_3–SiO_2 (31, 33) have been examined in the literature for alkanes isomerization, hydrotreatment, or CO + NO reactions. These studies demonstrated the complexity of these materials

[1] To whom correspondence should be addressed. Fax: +33/03 88 13 69 61. E-mail: bigeyc@ecpm.u-strasbg.fr.

[2] WO_3 will be used generically to refer to WOx surface groups although the structures are different from polycrystalline WO_3 powder.

0021-9517/01 $35.00

(nature, dispersion, stability and interaction of active phases on the support, etc.) and consequently the importance of the W loading, preparations and treatments which strongly influence the nature of tungsten species at the surface and thus the catalytic activities. Indeed, in the literature, it has been shown that for submonolayer systems, a tungsten oxide phase was present as an amorphous surface complex consisting of polymeric W species (W octahedrally coordinated) or mono- or dimeric species (W tetrahedrally coordinated). Above monolayer coverage, WO_3 aggregates were observed.

To stabilize a tungsten oxide phase, we settled on the use of CeO_2 as support, known for its basic and redox properties. We have prepared 9 wt% WO_3/CeO_2 and 0.9 wt% Pd/WO_3–CeO_2 materials, never employed in any application to our knowledge, as potential catalysts for reforming applications. In the present paper, we focused our attention on the physicochemical characterizations of such materials by means of N_2 adsorption, X-ray diffraction (XRD), Raman spectroscopy, and TPR. The nature of tungsten species deposited on ceria was studied and we explored to what extent calcination and reduction treatments could produce structural modification of W species. The characterizations of Pd/Al_2O_3, Pd/CeO_2, and Pd/WO_3 catalysts used as references for the catalytic properties of palladium are included in this part. The second part of this paper will be devoted to the catalytic properties of the WO_3/CeO_2 and Pd/WO_3–CeO_2 formulations which are active for skeletal rearrangements with very high selectivity in isomerized products and resistant to poisoning by carbonaceous residues. Relationships between activity and surface states of the catalysts (observed by XPS) will be exposed.

2. EXPERIMENTAL

2.1. Catalyst Preparations

A 9.1 wt% WO_3–CeO_2 material was prepared by impregnating ceria (Rhone Poulenc, specific surface area 115 m^2/g, porous volume 0.45 cm^3/g), using an equilibrium adsorption technique described by Baker and Clark (6) for WO_3/Al_2O_3 catalysts. $Na_2WO_4, 2H_2O$ salt (Merck, puriss 99%) was used as the tungsten precursor. Considering the net pH at the point of zero charge for ceria (6.75) and in order to allow the adsorption of tungsten anionic species, such as oxoanions, the tungstate solution (39.8×10^{-2} mol/l) was acidified by HNO_3 down to a pH equal to 4. The tungstic acid solution so obtained (H_2WO_4) was then added dropwise to CeO_2 under continuous stirring. The concentration and volume of tungstic solution were determined in order to obtain more than 10 wt% of WO_3 in the final samples. The excess solvent was evaporated on a hotplate. The powder obtained was dried at 120°C and then submitted to successive washings by diluted HNO_3 solution to eliminate residual Na^+ ions. The powder was finally dried at 120°C. The catalyst containing palladium was prepared by wetness impregnation of the WO_3/CeO_2 support previously calcined (400°C in air) for 4 h. An appropriate amount of acetyl acetonate of palladium(II) ($Pd(C_5H_7O_5)$ supplied by Strem Chemicals) solution was used in order to obtain ~1 wt% of Pd in the final sample. After solvent evaporation and drying at 110°C, the powder was calcined (400°C in air) for 4 h.

TABLE 1

Palladium, Tungsten, Residual Chlorine, and Remaining Sodium Contents in the Catalysts

Catalysts	Pd (wt%)	Cl (wt%)	W (wt%)	Na (wt%)
Pd/Al_2O_3	0.89	0.84	—	—
Pd/CeO_2	0.94	0.56	—	—
Pd/WO_3	0.87	560 ppm	—	—
WO_3–CeO_2	—	—	7.2	1.1
Pd/WO_3–CeO_2	0.93	—	6.3	1.1

Pd/WO_3, Pd/CeO_2, and Pd/Al_2O_3 catalysts, ~1 wt% Pd loading, were prepared as references. The Pd/WO_3 catalyst was prepared as described previously (23) by using a $Pd(NH_3)_4Cl_2$ precursor and WO_3 (Strem Chemicals, specific surface area 1.5 m^2/g, puriss 99.9%), previously calcined overnight. Pd/CeO_2 and Pd/Al_2O_3 catalysts were prepared by using the same method. Prior to impregnation, ceria was calcined at 550°C for 5 h and Al_2O_3 (Rhone Poulenc, gamma GC064, 206 m^2/g, porous volume 0.54 cm^3/g) was only dried at 110°C overnight. After impregnation by the Pd salt, the samples were calcined at 400°C for Pd/WO_3 and at 350°C for Pd/CeO_2 and Pd/Al_2O_3. Weight percentages of Pd, W, residual Cl, and remaining Na obtained by atomic absorption are reported in Table 1.

2.2. Catalyst Characterizations

Specific surface areas. N_2 adsorption isotherms at 77 K for the determination of surface areas were carried out in an automatic Coulter SA 3100 BET apparatus. Standard pretreatment was used prior to measurements and consisted of outgassing under vacuum at 350°C for 1 h. Surface measurements were conducted on fresh catalysts and catalysts treated *ex situ* in H_2 at 350°C (LTR) and 600°C (HTR) for 15 h. The specific surface area values were determined following the BET method.

XRD. X-ray diffraction spectra were recorded using a Siemens D5000 diffractometer with Cu$K\alpha$ radiation and a scanning rate of 0.02°/s in the 20–90° 2θ range. The spectra were recorded after *ex situ* LTR and HTR treatments.

Raman spectroscopy. Laser Raman spectra were collected in the 200–1200 cm^{-1} wavenumber range using a Perkin Elmer spectrometer 2000 NIR-FT-Raman apparatus equipped with a Nd:YAG laser source. The excitation

line of the laser was 1064 nm. The incident radiation used was in the range 30–600 mW, depending on the samples. The spectrometer resolution employed was 2 cm^{-1} (step 0.5). Self-supporting wafers were obtained from 50–120 mg samples pressed under 5 tons/cm^2. The spectra of crystalline CeO_2, WO_3, and Na_2WO_4 were recorded as references. For *in situ* treatments, the wafers were placed in a Pyrex cell which was then fixed on the equipment, allowing us to make treatments under gas flow (purified by gas clean filters) and controlled temperature. After each treatment, the cell was cooled to room temperature, isolated to prevent any contamination, and then introduced into the Raman spectrometer. Samples were studied as-prepared, and then after dehydration (vacuum at 200°C for 10 h). Reduction was carried out in hydrogen (flow 50 cm^3/min) at 350°C (10°C/min) for 5 h (LTR/5 h) followed by oxidation in oxygen at 400°C for 2 h (O400/2 h) and a new reduction at 350°C for 5 h. The parameters have been optimized for each sample by varying the sample weight, laser power, and scan numbers in order to obtain, as much as possible, well-defined tungsten bands. The Raman spectra of the Pd/WO_3–CeO_2 sample after *in situ* treatments are not presented (the sample is sensitive to laser beam exposure).

TPR. Temperature-programmed reduction analyses were done in an XSORB (IFP) apparatus described in Ref. (23). CeO_2, Al_2O_3, Pd/Al_2O_3, and Pd/CeO_2 materials were pretreated *in situ* in pure oxygen (25 cm^3/min) at 400°C (10°C/min) for 2 h. Before introduction of the reducing agent, a purge under Ar for 10 min was made. Finally, the temperature was raised to 900°C (600°C for Al_2O_3 and Pd/Al_2O_3) at 8°C/min in 1.03% H_2/Ar (25 cm^3/min). WO_3, Pd/WO_3, WO_3–CeO_2, and Pd/WO_3–CeO_2 samples were studied under similar conditions but without pretreatment and using a 5% H_2/Ar mixture as the reducing agent. The temperature was raised from room temperature to 900°C and maintained for 2 h (TPRa). The sample was then cooled to room temperature and oxidized under O_2 at 400°C for 2 h. After the sample was cooled to room temperature, a new TPR cycle was performed (TPRb). Three successive TPR cycles (TPRa, TPRb, TPRc) were then recorded as previously described (23).

3. RESULTS AND INTERPRETATION

3.1. BET

The specific surface areas (BET surface) for the as-prepared catalysts, after low- and high-temperature reduction, are given in Table 2. Large differences are observed between the catalysts depending on the treatment as compared to the initial surface areas of the supports (i.e., Al_2O_3, 206 m^2/g; CeO_2, 110 m^2/g; WO_3, 1.5 m^2/g). Specific surface areas of the catalysts are slightly lower than the initial surfaces of the supports except in the case of the Pd/WO_3 catalyst. In that case, we observe an increase in the BET surface probably resulting from the pretreatment of WO_3. Indeed, WO_3 was calcined at 400°C overnight before its use and we cautiously ascribe the increase in the BET surface to evacuation of the water molecules. Reduction at moderate temperature (350°C) leads to a small decrease in the BET surface area. Reduction at 600°C results in a marked decrease in the BET surfaces for samples containing ceria, from 85 to 7 m^2/g for Pd/WO_3–CeO_2 for example. We investigated the reversibility of the phenomena on the Pd/CeO_2 sample by measuring the BET surface after the following successive treatments: HTR + O400 + LTR. The value obtained (25 m^2/g) led us to conclude that the loss of surface was irreversible and was due to CeO_2 sintering. Such a phenomenon is characteristic of high specific surface areas and linked to thermal treatment, partly depending on the atmosphere, in our case reductive. Indeed, Laachir and co-workers (34, 35) showed a textural evolution of pure CeO_2 (same material as employed in this work, supplied from Rhone-Poulenc) as a function of temperature in any atmosphere (H_2, air, CO, vacuum). They noted a drastic decrease in the BET surface which was accelerated under H_2. After reduction at 550°C, the value of the BET surface of CeO_2 (initially 115 m^2/g) is above 30 m^2/g. The loss of surface was attributed to ceria sintering which proceeds first via the elimination of the microporosity. This phenomenon is accelerated under H_2 following the decomposition of residual carbonates species. Their elimination allows a higher mobility of ionic species followed by the growth of crystallites. Under H_2, reduction of CeO_2 occurs leading to oxygen vacancies, favoring the mobility of ionic species and thus sintering. This explanation is in good agreement with our experimental results.

TABLE 2

Surface Specific Areas (BET) as a Function of the Treatments

Catalysts	BET (m^2/g)		
	As prepared	LTR	HTR
Pd/Al_2O_3	205	200	184
Pd/CeO_2	102	96	23
Pd/WO_3	7	8	6
WO_3–CeO_2	85	79	7
Pd/WO_3–CeO_2	80	62	10

3.2. XRD Measurements

Table 3 summarizes the different phases obtained before and after *ex situ* LTR and HTR treatments for the various catalysts.

Cerium oxide diffraction lines. We observe the characteristic diffraction lines of CeO_2 fluorite structure for Pd/CeO_2, WO_3–CeO_2, and Pd/WO_3–CeO_2 catalysts at any temperature of reduction. We never observed diffraction peaks corresponding to a CeO_{2-x} composition, which is due

TABLE 3

Phases Identified by XRD on Catalysts as a Function of the Treatments

Catalysts	Treatments	Identified phases
Pd/Al_2O_3	As prepared, LTR, HTR	Al_2O_3
Pd/CeO_2	As prepared, LTR, HTR	CeO_2[a]
Pd/WO_3	As prepared	WO_3[b]
	LTR	$W_{20}O_{58}$[c]
	HTR	α-W[d]
WO_3–CeO_2	As prepared, LTR, HTR	CeO_2
Pd/WO_3–CeO_2	As prepared, LTR, HTR	CeO_2

[a] CeO_2 fluorite fcc (JCPDS 34-0394).
[b] WO_3 (JCPDS 5-0363).
[c] $W_{20}O_{58}$ (JCPDS 30-1387).
[d] α-W cc (JCPDS 4-0806).

to a rapid reoxidation to its normal stoichiometry. After reduction at 600°C, we noticed a decrease in the width of the diffraction peaks which can be attributed to a lower crystallinity of the materials compared with the initial samples. In the case of the WO_3–CeO_2 sample, it is interesting to note that the width of the peaks is reduced by 50%. The phenomenon is slightly smaller for the Pd/WO_3–CeO_2 sample. This can be due to palladium which prevents to a certain extent the ceria sintering. The results agree with the BET surface measurements.

Tungsten oxide diffraction lines. Reduction at 350°C of the Pd/WO_3 sample leads to the well-identified $W_{20}O_{58}$ phase. Further reduction at 600°C results in the formation of tungsten metal. No diffraction peaks due to tungsten species are observed for WO_3–CeO_2 and Pd/WO_3–CeO_2 samples at any temperature of treatment. The result could not be attributed to the tungsten loading which is above 6–7 wt%. Indeed accurate XRD analysis requires generally 4 wt%. This suggests that tungsten oxide species are mainly amorphous, well-dispersed in a thin layer or as small crystallites (<40 nm). The lack of detection of crystalline WO_3 is in full agreement with previous studies on WO_3–TiO_2 (36), WO_3–MgO (37), and WO_3–Al_2O_3 (2, 18, 38–40). Vermaire and Van Berge (18) have proposed from Raman spectroscopy experiments the existence of small crystallites on WO_3/Al_2O_3 catalysts for 10 to 17 wt% W loadings corresponding to 0.5–1 monolayer coverage. However, in most cases, to explain the absence of WO_3 reflection peaks, some authors have proposed that, above one monolayer coverage, tungsten was present as polymeric species in an octahedral environment or as isolated species in an octahedral or tetrahedral environment. In our case, we made a tentative calculation to evaluate the tungsten coverage corresponding to 7.2 wt% W for the WO_3–CeO_2 sample. We have considered the number of accessible oxygen atoms in the surface taking into account the (110) face of the FCC CeO_2 structure. Thus the corresponding oxygen ion concentration is 5.1×10^{18} O^{2-} ions/m^2 (5.6×10^{20} ions O^{2-}/g) considering the ceria surface. Taking into account the hypothesis of Hercules and co-workers on WO_3/Al_2O_3 (40), that one tungsten atom is chemically bound to two oxygen atoms (hydroxyl groups) of the support (1 : 2 stoichiometry), we obtain above 0.8 equivalent monolayer (Scheme 1a). One monolayer coverage would be reached for a 9 wt% W loading. Vermaire and Van Berge have considered for WO_3/TiO_2 (18) that during the adsorption step, a reaction occurred between tungsten species and one hydroxyl group of the titania surface (1 : 1 stoichiometry) (Scheme 1b). A subsequent reaction with the adjacent bridged hydroxyl group upon calcination would take place. According to this hypothesis, we obtain 0.4 equivalent monolayer. It is clear that the W–O and Ce–O (and Ce–Ce) bond lengths (approximately in the 2–2.4 Å range) partly determine the stoichiometry of the adsorption. However, the stoichiometry of adsorption is also a function of the tungsten oxoanions present in the aqueous solution during the preparation depending on various parameters (tungsten precursor, concentration, pH, and equilibrium time). But the most important parameter determining the surface W concentration and W structure is the point of zero charge (pzc) of the CeO_2 surface, which is strongly influenced by the presence of additional ions (H^+, Na^+, Cl^-) in contact with the surface. These ions are usually strongly bound to the surface. This can explain the remaining Na^+ in the WO_3/CeO_2 and $Pd/WO_3/CeO_2$ samples (Table 1). Thus, it is probable that the Na^+ ions decrease the number of W adsorption sites. Therefore, at this stage we have not enough information to determine the stoichiometry of adsorption but we can speculate that the tungsten coverage remains probably lower than one theoretical monolayer coverage.

3.3. Raman Investigations

Reference compounds. The Raman spectra of the CeO_2, Na_2WO_4, and WO_3 crystalline materials are presented in

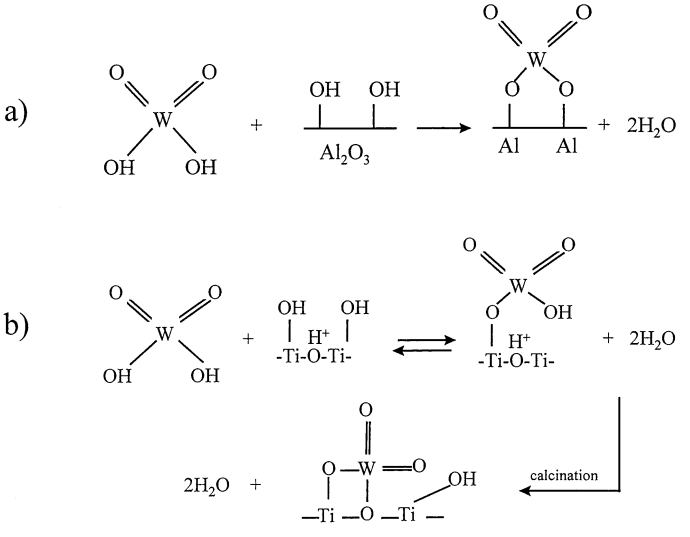

SCHEME 1

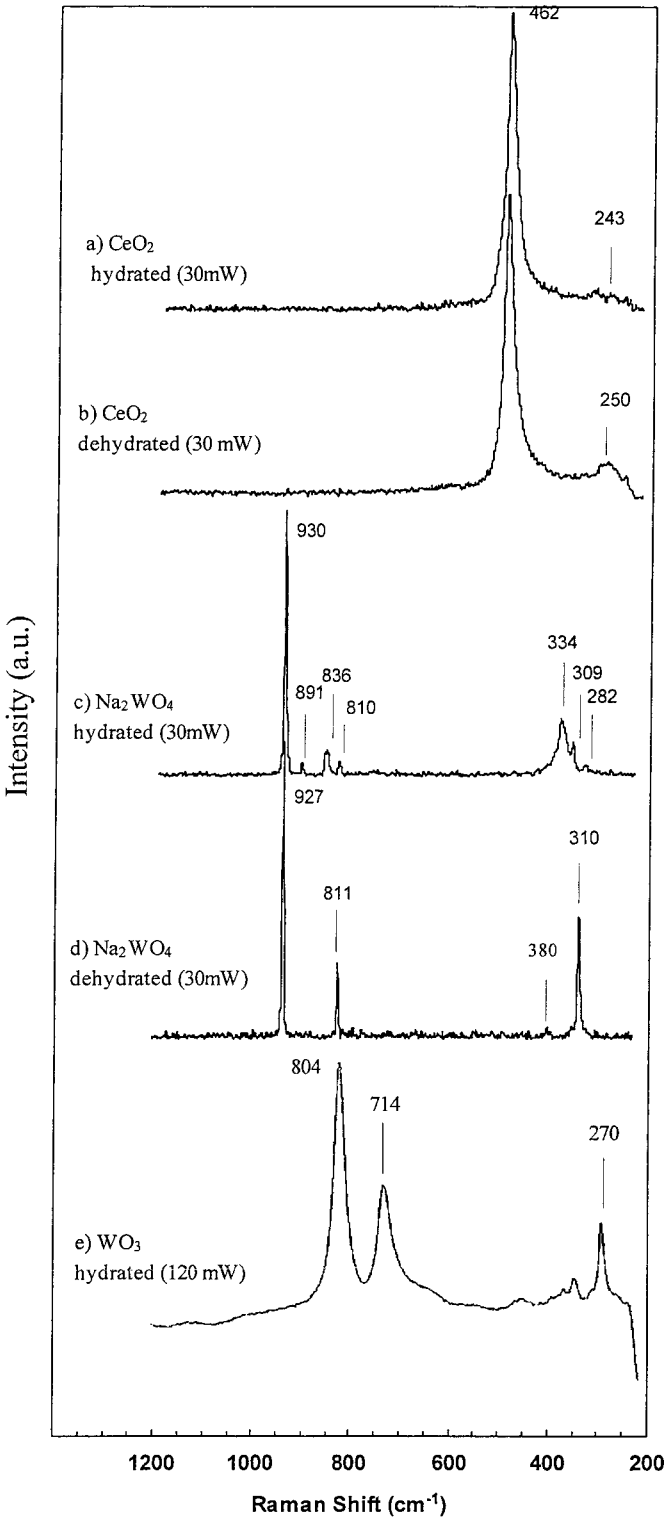

FIG. 1. Raman spectra of the references: CeO_2, Na_2WO_4, and WO_3.

Fig. 1. The Raman spectra of CeO_2 in the hydrated or dehydrated state (Figs. 1a, 1b) present a strong band at 462 cm^{-1} which is characteristic of fluorite type structure (F_{2g} mode) according to the literature (41, 42). The crystalline Na_2WO_4 spectrum recorded under ambient conditions (exposure in air atmosphere) exhibits a sharp band at 930 cm^{-1} and three smaller bands at 891, 836, and 810 cm^{-1}. A broad peak also appears around 334 cm^{-1} and a shoulder at 309 cm^{-1}. After dehydration, the spectrum is well resolved and shows three main sharp bands positioned at 927, 811, and 310 cm^{-1} with a smaller contribution at 380 cm^{-1}. The bands at 927 and 811 cm^{-1} are due to symmetric (A_1 mode) and antisymmetric (F_2 mode) W–O stretching vibrations, respectively according to data reported in the literature (38, 43, 44). The bands at 380 and 310 cm^{-1} correspond to W–O bending vibrations (F_2, E modes). The crystalline Na_2WO_4 has a spinal structure with tetrahedral site symmetry. Consequently, the stretching frequency at 927 cm^{-1} is commonly used to characterize WO_4^{2-} tetrahedral isolated species. The additional peaks at 891, 836, 334, and 282 cm^{-1} observed under ambient conditions are probably due to a lowering of symmetry, induced by some distortion of the WO_4 structure. This phenomenon probably results from hydration under wet atmosphere or impurities. Indeed, it is well known that a slight distortion of the ideal tetrahedron [WO_4] unit leads to a shift position which is ascribed to modifications of bond orders increasing the number of possible fundamental active Raman modes ($3N$-6) as has been observed for $CaWO_4$ material (43). Crystalline WO_3, possessing a distorted ReO_3 structure, is made up of distorted corner-shared WO_6 groups. The Raman spectrum (Fig. 1e) exhibits three major bands located at 804, 714, and 270 cm^{-1}, assigned to W–O stretching vibration modes (A_{1g}, E_g) and W–O–W deformations (F_{2g} mode). A comparison of the Na_2WO_4 and WO_3 references clearly shows the difference between the structures composed by [WO_4] or [WO_6] units. The position of the highest Raman band is observed at a higher wavenumber in the case of tetrahedral WO_4 groups (930 cm^{-1}) as compared to octahedral [WO_6] units (804 cm^{-1}). Indeed, in general, the position of the "W–O" stretching frequency vibration varies according to the W–O bond length (W–O bond order) (38, 44). However, the position of the highest "W–O" stretching Raman band could not be considered as a fingerprint to specify the nature of polyhedral structure especially in the case of supported materials. Distortion of polyhedra groups can lead to a significant increase in the W–O bond order which complicates the distinction based on the band positions between [WO_4] and [WO_6] units.

Raman spectra of WO_3–CeO_2 and Pd/WO_3–CeO_2 catalysts under ambient conditions. No data were reported in the literature related to WO_3–CeO_2 materials. In order to achieve an interpretation of the present results, we have compared them to those reported for "WO_3" supported on Al_2O_3, SiO_2, TiO_2, MgO, or ZrO_2. (Table 4). Raman spectra of WO_3–CeO_2 and Pd/WO_3–CeO_2 exhibit a most intense band between 400–500 cm^{-1} range centered at 460 cm^{-1}, characteristic of crystalline CeO_2 (Fig. 2). For a better

TABLE 4

Raman Bands Reported in the Literature for the Various Tungsten Oxide Species

Materials	References	Bands positions of main vibration modes (cm^{-1}) W=O stretching	W–O stretching	W–O bending	W–O–W deformation	Structures
WO_3–SiO_2	[43][c], [46][a], [47][b]		800–798	715–706	266–271	Crystalline WO_3
	[43][c]	927; 811			311	Td distorted [WO_4] units
	[47][b]	984*				Mono-oxo species
WO_3/TiO_2	[36][a], [48][b]		806–800			Crystalline WO_3
	[36][a], [48][b]	980–960			550, 215	Two-dimensional [WO_6] units
	[48][b]	1010*				Highly distorted Oh [WO_6] units
WO_3/Al_2O_3	[46][b], [49, 50][b]		806–801	713–693	268	Crystalline WO_3
	[46][b]	1005*				Mono-oxo tungsten oxide
	[49, 50][b]				580, 210	Polymeric tungsten oxide species
	[74][b], [46][b], [49, 50][b]	990–951 (1010*); 910–880		325–330	250	Td distorted [WO_4] units
WO_3/ZrO_2	[29][b], [46][b], [51][b]		809–804	718–713	274–260	Crystalline WO_3
	[46][b]		875	804		Polytungsten oxide species
	[51][b]	988	938	840		Small WO_x oligomeric clusters
	[52][b]	990 (1010*); 930				Monomeric WO_4^{2-}
	[29][b], [46][b]	1001*–1020				Mono-oxo tungsten species (Oh)
WO_3/MgO	[47]	1050; 980				[WO_4] units
	[46][b]		895, 817, 390, 330			$Mg_x(WO_4)_y$ $Ca_x(WO_4)_y$
	[46][b]		915, 330, 217			Crystalline $CaWO_4$
	[46][b], [47]		1050, 980, 915–909, 800–793			Crystalline $MgWO_4$

[a] Tungsten precursor $(NH_4)_{10}$ $H_2(W_2O_7)_6$.
[b] Tungsten precursor $(NH_4)_6$ H_2 W_{12} O_{40}.
[c] Tungsten precursor $(NH_4)_{10}$ $H_2(W_2O_7)_6 + NaNO_3$.
* Symbolizes dehydrated conditions. Td, tetrahedral; Oh, octahedral.

visualization of the signal in the 750–1100 cm^{-1} range caused by the tungsten oxide species, the spectra have been magnified (original magnification factor of 10). In neither case did we observe the characteristic bands (800, 715, and 270 cm^{-1}) ascribed to crystalline WO_3 oxide. Bands at 925 and 800–807 cm^{-1} attributed to tungsten species are observable and are consistent with tetrahedral [WO_4] units. Indeed, these bands are similar (positions and relative intensity) to those observed for the Na_2WO_4 reference (W–O stretching) and are close to those reported for monomeric WO_4^{2-} species in solution (W=O stretching) (52). These assignments agree with the previous results obtained on Na_2WO_4/CeO_2 material (53) and on WO_3–SiO_2 material prepared with an aqueous solution of paratungstate and $NaNO_3$ (43). However, we note a downshift of the W=O stretching frequency by comparison with a classical WO_3/Al_2O_3 (49, 50) which corresponds to an increase in the W=O bond length. Ostromecki *et al.* (49, 50) have reported a lowering of the W=O symmetric stretching frequency (~33–55 cm^{-1}) in the case of WO_3/Al_2O_3 promoted by metal oxide additives and precisely in the case of Na_2O. This result is consistent with the remaining Na in WO_3/CeO_2 sample. Two other bands are observed at 600 and 275 cm^{-1}. This spectral region is generally explored to study the vibration modes due to the presence of W–O–W linkages, a fingerprint for polymeric W species octahedrally coordinated. The band at 275 cm^{-1} is assigned to W–O–W deformation and is consistent with the band located at 600 cm^{-1} due to symmetric stretching of W–O–W linkages (44, 46, 49, 50). A W–O–W bond would be expected

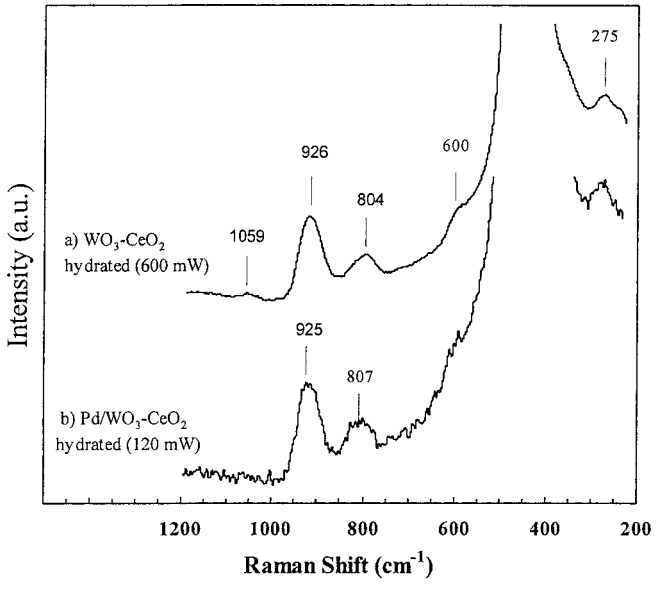

FIG. 2. Raman spectra of the WO_3–CeO_2 and Pd/WO_3–CeO_2 under ambient conditions.

to exhibit antisymmetric stretching in the 700–800 cm^{-1} region which would be detectable considering the intensity of the symmetric stretching. Consequently, we attribute the W–O–W bands to the presence of some tetrahedral species in a dimeric state as proposed previously for 10 wt% WO_3/Al_2O_3 (44). In addition, the WO_3/CeO_2 spectrum reveals another weak, broad, and poorly resolved band at about 1060 cm^{-1}. This frequency, not previously reported in the literature, is tentatively ascribed to carbonate species present in the CeO_2 support (34, 35) in accordance with the fact that they are no longer observed in the Pd/WO_3–CeO_2 sample which was calcined during the preparation. Palladium addition does not lead to structural changes in W species.

Raman spectra of WO_3–CeO_2 under in situ conditions (Fig. 3). For clarity's sake, the spectra have been magnified (factor of 4). Dehydration of the WO_3–CeO_2 sample (Fig. 3a) leads to the appearance of a new band at 969 cm^{-1} and the band at about 800 cm^{-1} seems to be composed of two overlapping bands centered at 829 and 797 cm^{-1}. The assignment of the band at 969 cm^{-1} is not straightforward. First, we can tentatively assign it to a mildly distorted W=O bond of the tungsten oxide species as proposed on 5–12 wt% WO_3/MgO showing a similar Raman band at 968 cm^{-1} (46). Additional bands in the Raman spectra of the Na_2WO_4/CeO_2 catalyst with increasing thermal treatment have also been observed and attributed to distortion of the ideal Td structures leading to a decrease of the symmetry (53). Second, we could suspect the formation of mono-oxo species. Kim *et al.* (47) have reported that the spectra of the *in situ* dehydrated WO_3/SiO_2 possess a single Raman band at 982–984 cm^{-1}, suggesting the presence of mono-oxo tungsten species. Salvati *et al.* (40) have assigned the band at 973 cm^{-1} observed for 10–15 wt% WO_3/Al_2O_3 to a W=O stretching mode of tetrahedral species. However, in most cases, mono-oxo species give Raman bands at higher frequencies, above 1000–1020 cm^{-1} (29, 46). Third, we could envisage a minor condensation of tetrahedral species leading to the formation of polymerized W species octahedrally coordinated. Ostromecki *et al.* (49) have reported that the Raman band (ambient condition) due to the symmetric stretching of the "W=O" bond sharpens and shifts from 951 to 975 cm^{-1} with increasing WO_3 loading from 1 to 25% as the ratio $[WO_6]$ to $[WO_4]$ increases. However, we have no additional evidence to conclude that polymeric W species are formed since no other changes are observed in the spectra. Moreover, in the present case, the W loading being constant and the specific surface area unchanged, the tungsten coverage is maintained. Under these conditions, we can hardly imagine a condensation of W species. A comparison of the Raman features under hydrated and dehydrated conditions confirms that tungsten species are not in the crystalline state such as Na_2WO_4 since the Raman bands would be sharper and remain unchanged (most crystal vibrations are unaffected by water (50)). After a reductive treatment at 350°C, the band at ~970 cm^{-1} sharpens. We note an increase in the relative intensity of the band at 800 cm^{-1} with additional bands at 696 and 356 cm^{-1} which could reflect the formation of poorly crystallized WO_3 or WOx clusters. The band located at 1100 cm^{-1} is probably due to an impurity contained in ceria. No major changes are obtained after a reoxidation at 400°C, followed by a new reduction at 350°C (Figs. 3c, 3d). The bands attributed to clusters or crystallites of WO_3 disappear and the spectra show features similar to those observed under dehydrated conditions. It is important to mention, considering the width of the bands, that we do not exclude the fact that the catalysts contain a broad distribution of various tungsten species having variable W–O bond orders.

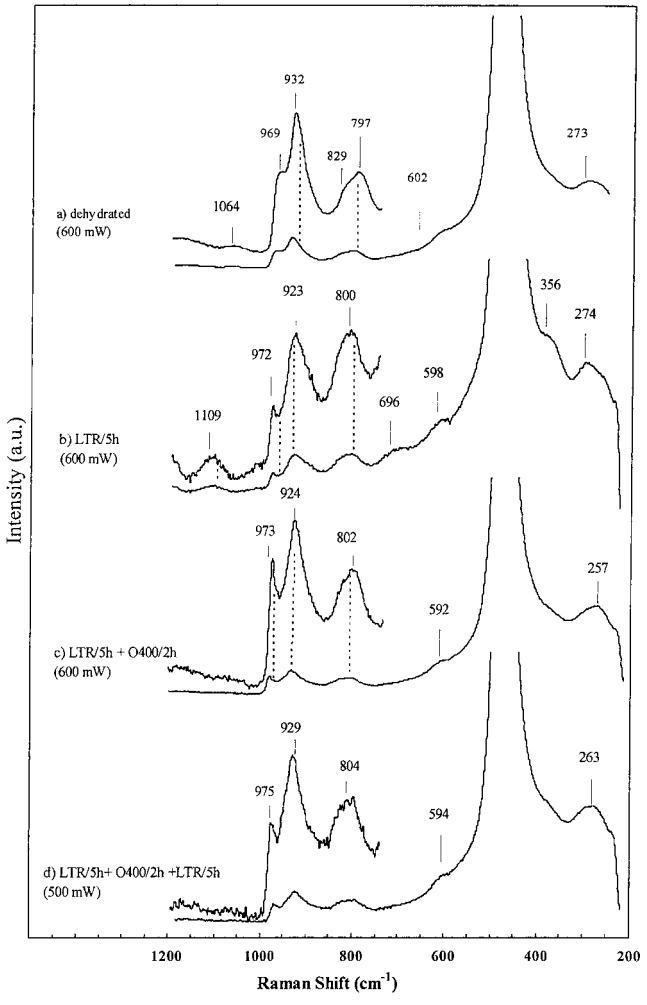

FIG. 3. Raman spectra of the WO_3–CeO_2 under *in situ* conditions: (a) dehydrated; (b) reduced in H_2 at 350°C for 5 h; (c) same as (b) and oxidized in air at 400°C for 1 h; and (d) same as (c) and reduced in H_2 at 350°C for 5 h.

3.4. Hydrogen TPR Analysis

Al_2O_3, CeO_2, and WO_3 bulk supports. The alumina profile is not reported because no consumption was noted up to 600°C. TPR patterns obtained for bulk CeO_2 and WO_3 supports are presented in Fig. 4. The reduction of ceria shows a small consumption at 261°C and two major consumptions with a maximum at 540°C and above 900°C, respectively. We can note a negative peak at 600°C. This profile is very similar to those obtained previously by Laachir *et al.* (34) and Yao and Yu Yao (54). The consumption peak at lower temperature is attributed to the reduction of the surface-capping oxygen (O^{2-} or O^- anions) and their contribution strongly depends on the initial specific surface area of CeO_2. The contribution beginning at 900°C is associated with the elimination of the O^{2-} anions of the lattice (reduction of the bulk). The negative peak is due to the desorption of carbonates present in the bulk of ceria according to the following reaction:

$$CO_3^{2-} + H_2(2H^+) \rightarrow CO_2 + H_2O. \qquad [1]$$

It is known that ceria can adsorb some quantities of H_2O and CO_2 at ambient temperature which are released under thermal treatment (34). The TPR profile obtained for WO_3 is more complicated and exhibits five peaks between 572°C and 900°C which were previously assigned to the reduction of $WO_3 \rightarrow W^0$ in several steps via WO_{3-x} sub-

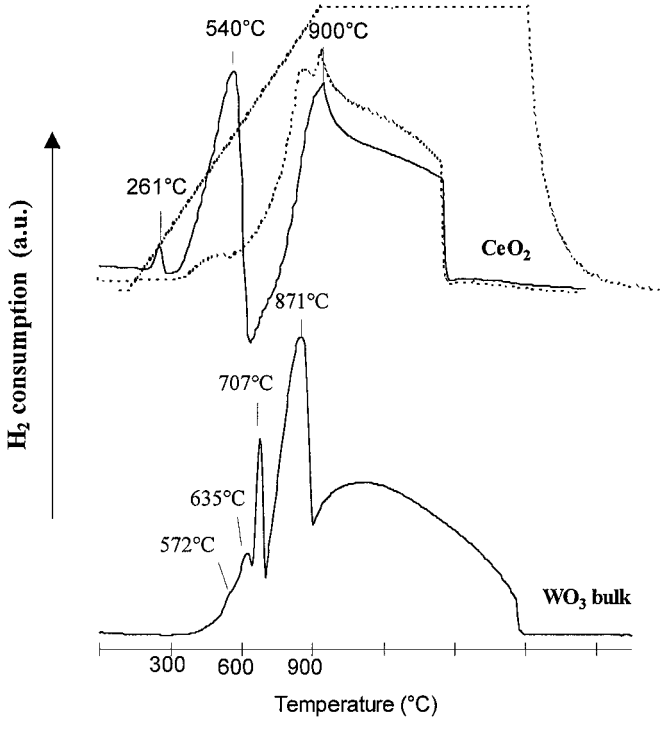

FIG. 4. TPR profiles for CeO_2 and WO_3 bulk supports (dashed line, second TPR cycle).

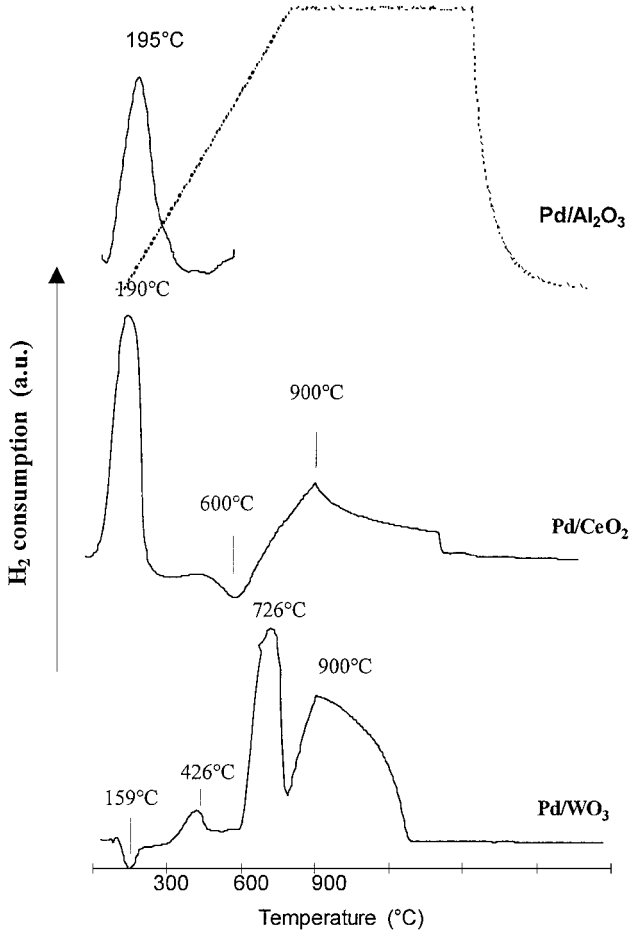

FIG. 5. TPR profiles for Pd/Al_2O_3, Pd/CeO_2, and Pd/WO_3 references.

oxides ($W_{20}O_{58}$, $W_{18}O_{49}$, $W_{24}O_{68}$) and WO_2 (23). The total hydrogen consumption (11.7×10^{-3} mol/g) corresponds to an almost complete reduction of WO_3 to tungsten metal (molar ratio $H_2/WO_3 = 2.7$).

Pd/Al_2O_3, Pd/CeO_2, and Pd/WO_3 as reference catalysts. Figure 5 gives the TPR results for reference compounds Pd/Al_2O_3, Pd/CeO_2, and Pd/WO_3. The Pd/Al_2O_3 profile shows a broad peak positioned at 195°C, assigned to the reduction of palladium oxide following the reaction

$$PdO + H_2 \rightarrow Pd + H_2O. \qquad [2]$$

The amount of H_2 consumed during the TPR (Table 5) corresponds to an incomplete reduction of Pd^{2+} to Pd^0 ($H_2/Pd = 0.63$). Some palladium oxide is probably reduced at ambient temperature (54) and not observable in our operating conditions. The Pd/CeO_2 system gives a TPR profile including the PdO reduction at 190°C, the carbonates decomposition at 600°C (negative peak), and the reduction of bulk CeO_2 around 900°C. The H_2 consumption at 190°C is much higher that necessary for the stoichiometric reduction of PdO. Moreover, we do not observe the peak at 540°C

TABLE 5

TPR Analysis for Bulk Supports and Pd/Al_2O_3, Pd/CeO_2, and Pd/WO_3 References

Samples	Total H_2 consumption (mol/g cat.)	T^0 (°C)	Assignments
CeO_2	1.34×10^{-3}	540	$CeO_{2\,surface} \rightarrow CeO_{2-x}$ ($VH_2 = 28.2 \times 10^{-5}$ mol/g)
		600	carbonates desorption
		900	$CeO_{2\,bulk} \rightarrow CeO_{2-x}$ ($VH_2 = 98.3 \times 10^{-5}$ mol/g)
WO_3	11.7×10^{-3}	572–900	$WO_3 + 3H_2 \rightarrow W^0$ via WO_{3-x} suboxides ($H_2/WO_3 = 2.7$)
Pd/Al_2O_3	5.20×10^{-5}	195	$PdO + H_2 \rightarrow Pd + H_2O$ ($H_2/Pd = 0.63$)
Pd/CeO_2	1.21×10^{-3}	190	$PdO + H_2 \rightarrow Pd + H_2O$ and $CeO_{2\,surface} \rightarrow CeO_{2-x}$ ($VH_2 = 39.5 \times 10^{-5}$ mol/g)
		900	$CeO_{2\,bulk} \rightarrow CeO_{2-x}$ ($VH_2 = 71.1 \times 10^{-5}$ mol/g)
Pd/WO_3	1.90×10^{-3}	426–900	$WO_3 + 3H_2 \rightarrow W^0$ via WO_{3-x} suboxides ($H_2/WO_3 = 2.8$)
		159	PdH_x decomposition

which was observed with pure ceria. This suggests that palladium promotes the reduction of CeO_2 surface to lower temperature. The peak at 190°C would be an overlapping of PdO and CeO_2 surface reduction in accordance with the H_2 consumption value obtained, 39.5×10^{-5} mol/g, which is close to the H_2 theoretical quantity: 8.8×10^{-5} (PdO reduction) + 28.2×10^{-5} (CeO_2 surface reduction). In the TPR profile of Pd/WO_3, three positive peaks are detected at 426, 726, and 900°C corresponding to the reduction of WO_3 in several steps as observed for bulk WO_3. The total H_2 consumption is close to the stoichiometric value 3 ($H_2/WO_3 = 2.8$). Comparing to results obtained on bulk WO_3, it appears that palladium facilitates the reduction of tungsten oxide via H_2 spill-over or formation/decomposition of a tungsten bronze (23). The negative peak at 159°C is attributed to a decomposition of palladium hydride formed at low temperature. No PdO reduction peak is observed. This species would be totally reduced at ambient temperature in the presence of WO_3.

WO_3–CeO_2 and Pd/WO_3–CeO_2 catalysts. As explained in Section 2, three successive TPRs were carried out on WO_3–CeO_2 and Pd/WO_3–CeO_2 samples. The profiles of the first TPR cycle (TPRa) for WO_3–CeO_2 and Pd/WO_3–CeO_2 are different from those obtained for bulk WO_3 and CeO_2 (Fig. 6). The analysis of the data is complicated by several

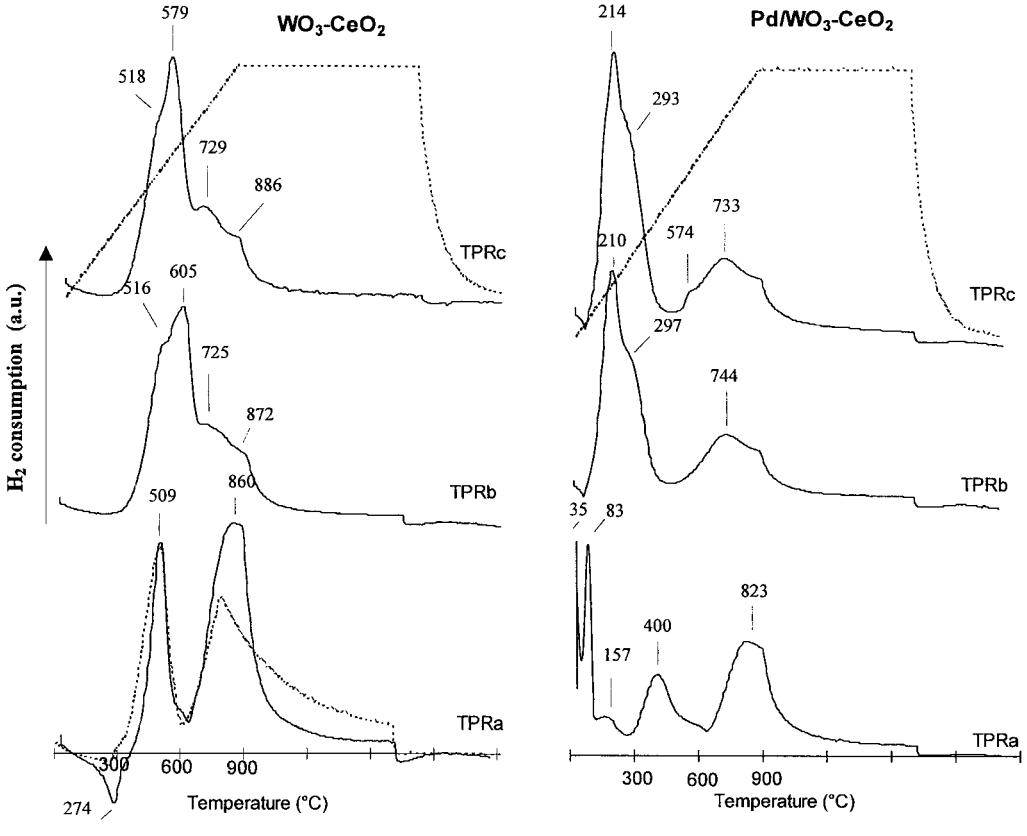

FIG. 6. TPR profiles for WO_3–CeO_2 and Pd/WO_3–CeO_2 catalysts obtained for three cycles (dashed line, reducing agent 1.03% H_2/Ar).

factors: CeO_2 itself undergoes reduction in the 500–900°C range which can lead to overlapping with tungsten species reduction (Fig. 4); dispersed tungsten species will not have the same reduction properties as their bulk counterpart; and metal–support interactions will modify the reduction of individual species. The difference in the way of reduction for the dispersed tungsten oxide species (two-dimensional structure) as compared to WO_3 (three-dimensional structure) is linked to the strong W–O bond with the oxide surface and the lack of nearest neighbors to share the reduced charge (55). Consequently, dispersed tungsten oxide species at low coverage will be reduced at higher temperatures than those required for bulk WO_3 crystallites as previously shown on WO_3/Al_2O_3 (1, 2, 8, 18, 20, 55), WO_3/TiO_2 (18), and WO_3/ZrO_2 (25, 56). In some cases, the reduction of tungsten species can be substantially hindered. A comparison of features with bulk WO_3 allows us to confirm that tungsten species are highly dispersed on the support and not in the crystalline form in which case we would observe the three characteristic steps of WO_3 reduction. The TPR pattern of WO_3–CeO_2 is composed of two main peaks above 509°C and 860°C and a shoulder at 600°C. The H_2 consumption (23×10^{-5} mol/g) and the maximum position for the band at 509°C are in good accordance with the reduction of the ceria surface (Table 6). The H_2 concentration does not seems to modify the TPR profile since a TPR done using a 1.03% H_2/Ar mixture is similar (included in Fig. 6 for comparison). The lower H_2 consumption by comparison with bulk CeO_2 (28×10^{-5} mol/g) is due to differences in surface areas which drop from 110 m^2/g to 85 m^2/g. As mentioned above, the surface reducibility strongly depends on the specific surface areas. The peak at 860°C could be attributed to the reduction of bulk ceria. However, it is not possible to quantify the theoretical H_2 consumption necessary to reduce ceria which can give various nonstoichiometric suboxides (CeO_{2-x}). This is why it is not excluded that this peak is partly due to dispersed species containing W in strong interaction with the support and thus hardly reducible. These species will be reduced in a single step: $W^{VI} \rightarrow W$ metal (18, 19). An intermediate reduction state seems unrealistic if we consider that isolated species contain oxygen linkages with CeO_2 support and no "reactive oxygen." Consequently, the charge created after the protonation of the accessible oxygen atom and water elimination could not be neutralized by a neighbor atom. The addition of palladium (0.93 wt%) to WO_3–CeO_2 weakly influences the reduction of WO_3–CeO_2 and the shape is maintained with supplementary peaks between 25°C and 250°C, ascribed to the reduction of Pd oxide species in interaction with the CeO_2 support (or tungsten species). At this stage, we do not have enough information to specify the Pd localization. Peaks at 400°C and 823°C correspond to the reduction of CeO_2 surface and CeO_2 bulk plus tungsten species, respectively. The maximum positions of the signals are lower than those observed for the Pd-free catalyst, showing here again that the metal improves the reduction process.

The second TPR cycles (TPRb) show a modification of the profiles as compared to the TPRa, irrespective of the catalyst. In the case of the WO_3–CeO_2 material, we do not observe the two distinctive peaks at 509°C and 860°C anymore but an overlapping of two peaks at 516°C and 605°C with an indication of a shoulder which seems to have two maxima above 729°C and 886°C. The total H_2 consumption is slightly higher than that obtained for TPRa (Table 6). The peak at the higher temperature is smaller than that for TPRa. This H_2 consumption decrease is in agreement with the loss of ceria surface area occurring after thermal treatment at 900°C under a reductive atmosphere as previously observed (35). We do not have the BET value after reduction at 900°C but in the case of reduction at 600°C, the BET is only 7 m^2/g (Table 2). Moreover, we have observed for

TABLE 6

TPR Analysis for WO_3–CeO_2 and Pd/WO_3–CeO_2 Catalysts

Samples	Cycles	Total H_2 consumption (mol/g cat.)	T^0 (°C)	Assignments
WO_3–CeO_2	TPRa	91×10^{-5}	509, 600	$CeO_{2\,surface}$ ($VH_2 = 23 \times 10^{-5}$ mol/g)
			860	$CeO_{2\,bulk}$ and WO_x species ($VH_2 = 68 \times 10^{-5}$ mol/g)
	TPRb, c	100×10^{-5}	516, 605, 725	WO_3 crystallites and/or $Ce_2(WO_4)_3$ reduction ($>VH_2^* = 64 \times 10^{-5}$ mol/g)
			725, 880	$CeO_{2\,bulk}$ and WO_3 crystallites ($VH_2^* = 38 \times 10^{-5}$ mol/g)
Pd/WO_3–CeO_2	TPRa	$>99 \times 10^{-5}$	35, 80, 157	$PdO \rightarrow Pd$ ($VH_2 > 23 \times 10^{-5}$ mol/g)
			400	$CeO_{2\,surface}$ ($VH_2 = 20 \times 10^{-5}$ mol/g)
			823	$CeO_{2\,bulk}$ and WO_x species ($VH_2 = 56 \times 10^{-5}$ mol/g)
	TPRb, c	97×10^{-5}	210, 293	WO_3 crystallites and/or $Ce_2(WO_4)_3$ reduction ($VH_2 = 67 \times 10^{-5}$ mol/g)
			733	$CeO_{2\,bulk}$ and WO_3 crystallites ($VH_2 = 30 \times 10^{-5}$ mol/g)

Theoretical H_2 consumption to reduce W^{6+} into W^0: 31×10^{-5} mol/g and 27×10^{-5} mol/g for WO_3–CeO_2 and Pd/WO_3–CeO_2 samples, respectively.
* Estimated values.

pure CeO_2 the almost complete disappearance of the peak due to the CeO_2 surface after two similar TPR cycles (see Fig. 4). Consequently, the peaks at 516 and 605°C are not due to ceria and we propose two suggestions. First, it is probable that these peaks are due to the reduction of small WO_3 crystallites, probably in two or three steps: $WO_3 \rightarrow W_{20}O_{58}$ (at 516°C), $W_{20}O_{58} \rightarrow WO_2$ (at 605°C), and $WO_2 \rightarrow W^0$ (at 725°C). W metal will be formed during the first TPR cycle (TPRa) and then after reoxidation at 400°C, the WO_3 crystallites could appear. Indeed, the ceria collapse goes with an increase in tungsten surface concentration due to a lower number of Ce^{4+} neighbors around W atoms. On the basis of a specific surface area equal to 7 m^2/g, the oxygen density at the surface is then 35.9×10^{18} O^{2-} ions/g, corresponding to 235×10^{18} W atoms/g (sample containing 7.2 wt% W). Taking into account the same hypothesis as in Section 3.2, the W coverage will be approximately between 6.5 and 13 equivalent monolayers (18, 40). At this coverage, it is likely that tungsten oxide is in the WO_3 crystallites state (or as polymeric tungsten species) as observed for the samples containing a tungsten coverage higher than the theoretical monolayer (1, 18, 28, 40, 44, 48). The small WO_3 aggregates will be more easily reducible than bulk WO_3. Indeed, the WO_3 reduction process is strongly influenced by the sample thickness (11, 18). A second possibility could be the formation of a mixed compound $Ce_2(WO_4)_3$ after the TPRa followed by the oxidation at 400°C by analogy with $Al_2(WO_4)_3$ formed under an oxidative atmosphere between 550–1100°C via a solid-state reaction between WO_3 and Al_2O_3 (14, 57) and $Ce_2(MoO_4)_3$ highlighted on MoO_3–CeO_2 (58). $Ce_2(WO_4)_3$ has been prepared by crystallization from a molten mixture of WO_3 and CeO_2 at 1550°C (59). According to the authors, the compound begins to be formed above 700°C via oxygen removal. The experimental H_2 consumption ($H_2/Ce_2(WO_4)_3 = 1.8$) is close to the theoretical value necessary to reduce $Ce_2(WO_4)_3$ by the following reaction:

$$Ce_2(WO_4)_3 + 2H_2 \rightarrow 2WO_3 + W^0 + 2CeO_2. \qquad [3]$$

The most striking difference when the sample contains palladium is that we obtain two well-separated peaks. The peak previously attributed to WO_3 crystallites or $Ce_2(WO_4)_3$ reduction is shifted toward lower temperatures. This confirms again that palladium improves the tungsten species reduction. No modifications are then observed on the last TPR (TPRc).

4. GENERAL DISCUSSION

The nature of tungsten oxide species in supported systems is controversial. In a wide range of W concentrations, isolated tetrahedral or octahedral species, di- or trimeric species, polymerized octahedral species, small clusters, or even WO_3 have been previously proposed. This is due to the complex mechanism of deposition of W^{6+} species from aqueous solution on a support, depending on various parameters: pzc and hydroxyl group reactivity of the support, pH and concentration of the impregnating solution, the nature of the W precursor, or the W loading. In the present study, the physicochemical characterizations of 9.1 wt% WO_3/CeO_2 and Pd/WO_3–CeO_2 catalysts led us to conclude that the deposited tungsten phase was not in a crystalline state and was well dispersed (XRD). We have suggested on the basis of Raman experiments that oxotunsgten species consisted of monomeric or dimeric species in which W was tetrahedrally coordinated. These species will be barely reducible as a result of their strong interaction with the CeO_2 support (TPR). In this part, we will examine to what extent the pH of aqueous tungsten species and the tungsten precursor (and W loading) could explain the present results. We will then examine the possible modifications induced by dehydration, calcination, or reduction steps.

4.1. *Influence of the pH*

The pH and concentration appear to be the most important factors in the genesis of tungsten species in the impregnating solution (18, 47, 50, 55, 56). The deposition of the W^{6+} species on the support takes place by adsorption of anionic species. In a wide range of concentrations and pH, the electrolytic solution could contain up to 12 species. It was proved that in the pH range 10–3.5 and in the concentration range 1×10^{-4}–2.5×10^{-2} M, only eight species were present (55). The most stable species formed from tungstate WO_4^{2-} acidification are the paratungstate-B $[H_2W_{12}O_{42}]^{10-}$ and the metatungstate $[H_2W_{12}O_{40}]^{6-}$, both resulting from the paratungstate-A $[W_7O_{24}]^{6-}$ transformation following equilibria [4], established very slowly (a few days or months at ambient temperature) (18, 50, 56, 60, 61):

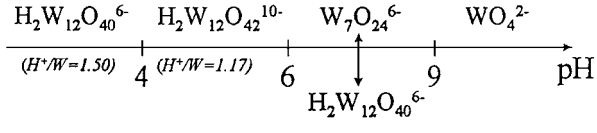

[4]

For the molybdate species, it is generally accepted that the extension to the hexacoordination is obtained at low pH values. Polyanions of W^{VI} are constituted by octahedral WO_6 units, strongly distorted (61). The terminal oxygens in WO_6 units are not very basic, which restricts the protonation and so prevents extensive polymerization. To perform anionic exchange on ceria (pH at pzc, 6.75), the tungstate solution was acidified down to a pH value above 4 for which the predominant species would be polytungstates. Taking into account the tungsten concentration in the starting aqueous solution and referring to Ostromecki *et al.* (40, 46, 50), $H_2W_{12}O_{40}^{6-}$ species would be mainly formed and polymeric species would be expected on the final WO_3–CeO_2 material. However, this conclusion is not consistent

with Raman experiments proving the existence of tetrahedral WO_4^{2-} species and is different from previous results assuming that the stable molecular structure of the dispersed oxide corresponds to the molecular species which prevail in solution equilibria at the pH corresponding to the net surface pH of the support at its point of zero charge. It is likely that the slow equilibrium between tungstates species and the ionic exchange should favor the adsorption of isolated oxoanions. Moreover, to envisage the adsorption of polyanionic species, a fair distribution of the reacting protonated hydroxyl groups on CeO_2 would be necessary. It appears that the tungstate deposition mechanism is not straightforward and cannot be simplified as Eq. [4] essentially based on pH and concentration of the starting material. A recent study proved that monomeric WO_4^{2-} species deposition on Al_2O_3 still remains considerable even in the pH range 3.5–5 (55) which was attributed to "the relatively low negative charge of the monomeric species and the negative potential developed at the IHP (inner Helmholtz plane)." By analogy with the mechanism of the W^{6+} species deposition proposed by Karakonstantis *et al.* (55), and taking into account our experimental conditions (pH 4, C = 0.04 M), we suggest a selective deposition of WO_4^{2-} species via an electrostatic adsorption (Eq. [5]) or via a reaction with one protonated hydroxyl group (Eq. [6]). In this case, the negative charge might be stabilized by neighboring H_2O^+ or neutralized by Na^+ acting as a countercation (remaining in the 1.1 wt% range).

$$Ce\text{–}OH_2^+ + WO_4^{2-} \rightarrow Ce\text{–}OH_2^+ \cdots WO_4^{2-}(Na^+) \quad [5]$$

$$Ce\text{–}OH_2^+ + WO_4^{2-} \rightarrow Ce\text{–}O\text{–}WO_3^-(Na^+) + H_2O. \quad [6]$$

4.2. Influence of the Precursor Salt

The choice of the starting material might have an influence on the type of tungsten species deposited at the surface. In the present study, Na_2WO_4, $2H_2O$ was used as the W precursor. We pointed out that the sodium was sill present and remained in relatively high quantity in the final samples (1.1 wt%). Washings with HNO_3 solution did not eliminate the residual sodium and 60% of Na^+ initially introduced remained on the catalysts which corresponds to a Na/W atomic ratio equal to 1.2 (initial Na/W ratio = 2). Similar observations were previously reported on WO_3/Al_2O_3 at 6 wt% W loading prepared with an aqueous sodium tungstate solution (16). The authors suggested that sodium impurities from alumina and tungsten precursor assisted in the formation process of irreducible species (i.e., tetrahedral species). No additional hypotheses were given to explain this phenomenon. It is well known that impurities such as alkaline earths could greatly influence and modify the catalytic properties of materials. For example, Tittarelli *et al.* (57) have observed an increase in the thermal stability of the surface in WO_3 supported on Al_2O_3 containing Ba^{2+} cations ($Ba(OH)_2$). In the same way, Kim *et al.* (46) have shown on WO_3/MgO that CaO or MgO impurities, soluble in water, could react with aqueous WO_4^{2-} species and produce nonstoichiometric $Ca_x(WO_4)_y$. Other convincing results were obtained on Na-doped MoO_3/TiO_2 (62) and WO_3/SiO_2 (43) materials. The authors reported that the addition of sodium decreased the reducibility of the supported phases, which was attributed to changes in the molybdenum or tungsten structure. The initial octahedral structure changes into distorted tetrahedral structure with Na addition and simultaneously the reducibility is inhibited in the latter case. The genesis by impregnation of tungsten–alumina-based catalysts was investigated by Pizzio *et al.* (63). The main result was that impregnated and calcined solids showed the predominant presence of the WO_4^{2-} monomeric species, regardless of the precursor used in the impregnating solution. The above considerations confirm that Na^+ is involved in the formation of tetrahedral tungsten species. In the present study, it must be stressed that Na^+ cations could be strongly adsorbed on the CeO_2 surface during the tungstate species deposition. In such a case, it is probable that the pH at the point of zero charge for CeO_2 is modified and that the number of accessible hydroxyl groups is reduced. We suggest that the Na^+ impurities allow us to maintain monomeric WO_4^{2-} species in tetrahedral coordination, interacting with the W=O bonds. This would explain the low W=O stretching frequency observed by comparing to those given in the literature for supported tetrahedral species. The stabilization of the excess negative charge of WO_4^{2-} by Na^+ explains the high stability of the tetrahedral species, highly reducible (TPR). The Na^+ cations, strongly adsorbed on the surface, could avoid to some extent the polymerization of the tetrahedral species. This is consistent with the fact that only a small condensation of W species is observed leading to dimeric species maintaining a tetrahedral coordination. We do not totally exclude the possibility that some tungsten species are maintained as "Na_xWO_y" (agglomerated in the ceria pores) as reported for Na_2WO_4/CeO_2 and Na_2WO_4/SiO_2 (43, 53). We exclude the localization of Na^+ in a tungsten bronze such as Na_xWO_3 which requires a three-dimensional network of WO_3 for Na^+ insertion. We have illustrated the oxotungsten species probably formed during the deposition, taking into account the role of sodium (Scheme 2). Species I would be formed following Eq. [5] and species IIa and IIb following Eq. [6]. After drying of the WO_3–CeO_2 material (110°C/air/overnight), species I may easily be converted to species II. Species III would be formed after dimerization of two adjacent species II.

4.3. Influence of Dehydration, Calcination, and Reduction Treatments

The Raman spectrum obtained after dehydration of the WO_3–CeO_2 sample showed a new sharp band at ~970 cm^{-1}. We discard the possibility of the formation of polymeric W

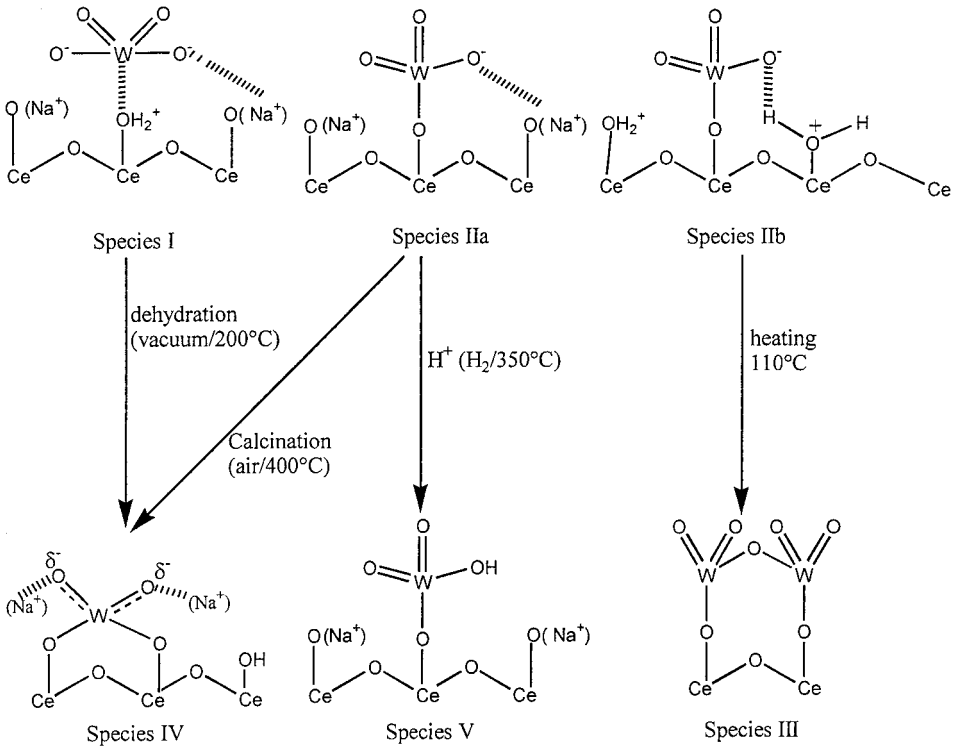

SCHEME 2

species. Indeed, we feel that a modification of the CeO_2 support is necessary to allow the polymerization of isolated tetrahedral W species. We argue that a dehydration treatment (vacuum/200°C) does not modify the specific surface area of the sample since a similar treatment is applied prior to BET measurements (outgassing/350°C). Moreover, ~970 cm^{-1} is too low a frequency to suppose the formation of mono-oxo W species, as compared to the literature data (1000–1020 cm^{-1}). Thus the most probable explanation would be the formation of distorted tetrahedral species. We propose that dehydration of species I and II leads to the formation of species IV (Scheme 2) via a new reaction with a hydroxyl group and the elimination of one water molecule. A puzzling result is however obtained after the reductive treatment at 350°C. Poorly resolved Raman bands characteristic of WO_3 crystallites appeared. This result is not consistent with the BET surface measurement which remains above 79 m^2/g and close to the initial value (85 m^2/g). Moreover, the bands ascribed to WO_3 are no longer observed after an oxidative treatment or a new reductive treatment. One may invoke a local heating under the laser beam. Reduction at 350°C or oxidation at 400°C did not seem to produce supplementary structural changes of the oxotungsten species. We rule out the possibility that a compound such as $Ce_2(WO_4)_3$ is formed in the same way as $Al_2(WO_4)_3$ can be formed on WO_3/Al_2O_3 (4, 50, 57). Temperatures above 1000°C are necessary to observe such compounds or longer exposures. Such crystalline tungstate compounds are generally formed consecutively with textural modifications of the supports, mainly sintering. In the case of CeO_2, temperatures above 500°C are required to observe changes in specific surface areas. We suggest that species V may be formed under reductive treatment after protonation of species II leading in that way to Brønsted acidic sites.

5. CONCLUSION

In this study, we dealt with the physicochemical characterizations of WO_3–CeO_2 and Pd/WO_3–CeO catalysts in order to clarify the nature of the deposited tungsten phase. Modifications which could be induced by dehydration, calcination, or reduction treatments were examined. The main conclusions from the present study are summarized as follows:

1. The tungsten phase on WO_3–CeO_2 and Pd/WO_3–CeO_2 catalysts (9.1 wt% WO_3) is well dispersed and contains mainly isolated tetrahedral species. The presence of such species in materials for which the tungsten loading approaches 0.8 equivalent monolayer is in good accordance with the conclusions previously given in the literature for WO_3–Al_2O_3 and WO_3–ZrO_2 materials.

2. The presence of monomeric and dimeric W species in the final samples is rather unexpected since the impregnating tungstate solution should contain mainly polymeric

species. The use of Na_2WO_4, $2H_2O$ as the tungstate precursor favors the formation of isolated WO_4^{2-} species.

3. We suggest that Na^+ ions strongly interact with ceria during the tungstate deposition which modifies the pH at the pzc and decreases the number of accessible sites for W species adsorption which prevents the formation of polymeric species.

4. We have proposed the existence of various tetrahedral species which are linked with one or two adjacent hydroxyl groups of the support. Tungsten is maintained in the W^{VI} state.

5. The tetrahedral species are highly stable. Na^+ cations strongly bonded to the support allow us to maintain the tungstate structure in the tetrahedral environment. No major modifications are induced by reductive or oxidative treatments at moderate temperatures (350–400°C). Dehydration and calcination lead to more tetrahedral species linked to a pair of hydroxyl groups. Reductive treatment would allow us to produce Brønsted sites.

6. Tetrahedral species are reduced at temperatures above 900°C in one step giving W metal, as a result of ceria sintering.

7. We suggest that the $Ce_2(WO_4)_3$ compound may be formed after a reduction at 900°C followed by an oxidation at 400°C.

ACKNOWLEDGMENTS

C. B. thanks Professor Su (CMI, Namur University, Belgium) for the use of the Raman spectrometer.

REFERENCES

1. Ramirez, J., and Gutierrez-Alejandre, A., *J. Catal.* **170**, 108 (1997).
2. Thomas, R., Van Obers, E. M., De Beer, V. H. J., Medema, J., and Moulijn, J. A., *J. Catal.* **76**, 241 (1982).
3. Lietti, L., Svachula, J., Forzatti, P., Busca, G., Ramis, G., and Breganic, F., *Catal. Today* **17**, 131 (1993).
4. Grunert, W., Shpiro, E. S., Feldhaus, R., Anders, K., Antoshin, G. V., and Minachev, K. M., *J. Catal.* **107**, 522 (1987).
5. Rodriguez-Ramos, I., Guerrero-Ruiz, A., Homs, N., Ramirez de la Piscina, P., and Fierro, J. L. G., *J. Mol. Catal. A: Chemical* **95**, 147 (1995).
6. Baker, B. G., and Clark, N. J., *Stud. Surf. Sci. Catal.* **30**, 483 (1987).
7. Gielgens, L. H., Van Kampen, M. G. H., Broek, M. M., Van Hardeveld, R., and Ponec, V., *J. Catal.* **154**, 201 (1995).
8. Benitez, V. M., Querini, C. A., Figoli, N. S., and Comelli, R. A., *Appl. Catal. A* **178**, 205 (1999).
9. Logie, V., Maire, G., Michel, D., and Vignes, J. L., *J. Catal.* **188**, 90 (1999).
10. Katrib, A., Logie, V., Saurel., N., Wehrer, P., Hilaire, L., and Maire, G., *Surf. Sci.* **30**, 754 (1997).
11. Logie, V., Wehrer, P., Katrib, A., and Maire, G., *J. Catal.* **189**, 438 (2000).
12. Ogata, E., Kamiya, Y., and Ohta, N., *J. Catal.* **29**, 296 (1973).
13. Haber, J., Stoch, J., and Ungier, L., *J. Solid State Chem.* **29**, 237 (1979).
14. Biloen, P., and Pott, G. Y., *J. Catal.* **30**, 169 (1973).
15. Wachs, I. E., Chersich, C. C., and Hardenberg, J. H., *Appl. Catal.* **13**, 335 (1985).
16. Chappell, P. J. C., Kibel, M. H., and Baker, B. G., *J. Catal.* **110**, 139 (1988).
17. De Angelis, B. A., and Schiavello, M., *J. Solid State Chem.* **21**, 67 (1977).
18. Vermaire, D. C., and Van Berge, P. C., *J. Catal.* **116**, 309 (1989).
19. Scheffer, B., Molhoek, P., and Moulijn, J. A., *Appl. Catal.* **46**, 11 (1989).
20. Kadkhodayan, A., and Brenner, A., *J. Catal.* **117**, 311 (1989).
21. Fouad, N. E., Attyia, K. M. E., and Zaki, M. I., *Powder Technol.* **74**, 31 (1993).
22. Bigey, C., Logie, V., Bensaddik, A., Schmitt, J. L., and Maire G., *J. Phys. IV Fr.* **8**, 553 (1998).
23. Bigey, C., Hilaire, L., and Maire, G., *J. Catal.* **184**, 406 (1999).
24. Bigey, C., and Maire, G., *J. Catal.* **196**, 224 (2000).
25. Barton, D. G., Soled, S. L., Meitzner, G. D., Fuentes, G. A., and Iglesia, E., *J. Catal.* **181**, 57 (1999).
26. Iglesia, E., Barton, D. G., Soled, S. L., Miseo, S., Baumgartner, J. E., Gates, W. E., Fuentes, G. A., and Meitzner, G. D., *Stud. Surf. Sci. Catal.* **101**, 533 (1996).
27. Hino, M., and Arata, K., *Appl. Catal. A* **169**, 151 (1998).
28. Comelli, R. A., Canavese, S. A., and Figoli, N. S., *Catal. Lett.* **55**, 177 (1998).
29. Vaudagna, S. R., Comelli, R. A., and Figoli, N. S., *Appl. Catal. A* **164**, 265 (1997).
30. Larsen, G., Lotero, E., Raghavan, S., Parra, R. D., and Querini, C. A., *Appl. Catal. A* **139**, 201 (1996).
31. M'Boungou, J. S., Schmitt, J. L., Maire, G., and Garin, F., *Catal. Lett.* **10**, 391 (1991).
32. Ouafi, D., Mauge, F., Lavalley, J. C., Payen, E., Kasztelan, S., Houari, M., Grimblot, J., and Bonnelle, J. P., *Catal. Today* **4**, 23 (1988).
33. Regalbuto, J. R., Fleisch, T. H., and Wolf, E. E., *J. Catal.* **107**, 114 (1987).
34. Laachir, A., Perrichon, V., Badri, A., Lamotte, J., Catherine, E., Lavalley, J. C., El Fallah, J., Hilaire, L., Le Normand, F., Quemere, E., Sauvion, G. N., and Touret, O., *J. Chem. Soc., Faraday Trans.* **87**(10), 1601 (1991).
35. Perrichon, V., Laachir, A., Abouarnadasse, S., Touret, O., and Blanchard, G., *Appl. Catal. A* **129**, 69 (1995).
36. Martin, C., Solana, G., and Rives, V., *Catal. Lett.* **49**, 235 (1997).
37. Martin, C., Malet, P., Rives, V., and Solana, G., *J. Catal.* **169**, 516 (1997).
38. Chan, S. S., Wachs, I. E., and Murrell, L. L., *J. Catal.* **90**, 150 (1984).
39. Scheffer, B., Heijeinga, J. J., and Moulijn, J. A., *J. Phys. Chem.* **91**, 4752 (1987).
40. Salvati, L., Makovsky, L. E., Stencel, J. M., Brown, F. R., and Hercules, D. M., *J. Phys. Chem.* **85**, 3700 (1981).
41. Groppi, G., Cristiani, C. C., Lietti, C., Ramella, C., Valentini, M., and Forzatti, P., *Catal. Today* **50**, 399 (1999).
42. Xu, Z., Yang, X. Y., Lunsford, J. H., and Rosynek, M. P., *J. Catal.* **154**, 163 (1995).
43. Wu, J., and Li, S., *J. Phys. Chem.* **99**, 4566 (1999).
44. Horsley, J. A., Wachs, I. E., and Brown, J. M., *J. Phys. Chem.* **91**, 4014 (1987).
45. Nakamoto, N., "Infrared and Raman Spectra of Inorganic Coumpounds," 3rd Ed. Wiley, New York, 1978.
46. Kim, Du S., Ostromecki, M., and Wachs, I. E., *J. Mol. Catal. A* **106**, 93 (1996).
47. Kim, Du S., Ostromecki, M., and Wachs, I. E., *Catal. Lett.* **33**, 209 (1995).
48. Vuurman, M. A., Wachs, I. E., and Hirt, A. M., *J. Phys. Chem.* **95**, 9928 (1991).
49. Ostromecki, M. M., Burcham, L. J., Wachs, I. E., Ramani, N., and Ekerdt, J. G., *J. Mol. Catal. A* **132**, 43 (1998).
50. Ostromecki, M. M., Burcham, L. J., and Wachs, I. E., *J. Mol. Catal. A* **132**, 59 (1998).
51. Scheithauer, M., Grasselli, R. K., and Knözinger, H., *Langmuir* **14**, 3019 (1998).

52. Gazolli, D., Valigi, M., Dragone, R., Marucci, A., and Mattei, G., *J. Phys. Chem. B* **101**, 11129 (1997).
53. Yu, Z., Yang, X., Lunsford, J. H., and Rosynek, M. P., *J. Catal.* **154**, 163 (1995).
54. Yao, H. C., and Yu Yao, Y. F., *J. Catal.* **86**, 254 (1984).
55. Karakonstantis, L., Matralis, H., Kordulis, Ch., and Lycourghiotis, A., *J. Catal.* **162**, 295 (1996).
56. Yori, J. C., Vera, C. R., and Parera, J. M., *Appl. Catal. A* **163**, 165 (1997).
57. Tittarelli, P., Ianibello, A., and Villa, P. L., *J. Solid State Chem.* **37**, 95 (1981).
58. Kuang, W., Fan, Y., and Chen, Y., *Catal. Lett.* **50**, 31 (1998).
59. Gressling, T., and Müller-Buschbaum, H., *Z. Naturforsch. b* **50**, 1513 (1995).
60. Baes, C. F., and Mesmer, R. E., "Hydrogenolysis of cations." Wiley, New York, 1996.
61. Pope, M. T., "Heteropoly and Isopolyoxometallates." Springer-Verlag, Berlin, 1983.
62. Martin, C., Martin, I., and Rives, V., *J. Catal.* **147**, 465 (1994).
63. Pizzio, L. R., Caceres, C. V., and Blanco, M. N., *Catal. Lett.* **33**, 175 (1995).